Flat-top optical filter via the adiabatic evolution of light in an asymmetric coupler

Xin-Biao Xu, Xiang Guo, Wei Chen, Hong X. Tang, Chun-Hua Dong, Guang-Can Guo, and Chang-Ling Zou

Flat-top optical filter via the adiabatic evolution of light in an asymmetric coupler

Xin-Biao Xu[1,2], Xiang Guo[3], Wei Chen[1,2], Hong X. Tang[3],

Chun-Hua Dong[1,2], Guang-Can Guo[1,2], Chang-Ling Zou[1,2*]

[1]*Key Laboratory of Quantum Information, University of Science and Technology of China, CAS, Hefei, Anhui 230026, China.*
[2]*CAS Center For Excellence in Quantum Information and Quantum Physics,*
University of Science and Technology of China, Hefei, Anhui 230026, China and
[3]*Department of Electrical Engineering, Yale University, New Haven, Connecticut 06511, USA.*

The flat-top optical filter is an important component in practical optical applications, but it is very challenging for experimental realization in the integrated photonic platform. Here, we propose a robust and high-efficiency optical filter with wide-band flat-top, based on the adiabatic conversion of light in coupled waveguides with a chirped modulation of the gap. The bandwidth of the filter can be 110 nm for telecom wavelengths, but owing to the adiabatic criteria, the length of the device is about 20 mm. To narrow the bandwidth and reduce the footprint of the device simultaneously, an additional apodization modulation of the geometry is introduced, and a 6 nm bandwidth can be realized with a device length of 4 mm. Besides, the influences of structure parameters on the device performance are also analyzed, and the results show that the device is robust to the variation of the structure parameters. The proposed integrated bandpass filter is feasible for experiments, thus it would be useful in both classical and quantum information processing on photonic chips.

I. INTRODUCTION

Great progress has been achieved in photonic integrated circuits (PICs) over the past decades [1, 2]. The PICs have shown great potential for scalable classical and quantum information processing [3–7]. Among various optical components, an optical filter is of great importance for signal processing. For example, it is necessary for dividing the signals into different wavelength channels, blocking the undesired stray lights, and separating the strong control laser from the weak signal for a nonlinear optics process, especially for the on-chip second-order nonlinearity processes [8] and optical comb [9], where the ultra-broadband optical signals are related. Accordingly, a wide-band and flat-top filter with high-efficiency is needed. For PIC, a number of schemes have been proposed to realize flat-top optical filters [10–12], such as the Mach-Zehnder interferometers [13], gratings [14], photonic crystal [15, 16] and cascade microring resonators [17, 18]. In these schemes, complex controls and high-precision fabrication processes are required, which makes the realization of flat-top filters challenging.

On the other hand, inspired by the similarity between state evolution in quantum mechanics and electromagnetic wave propagation in optics, photonic platform has been used for studying the quantum effects, including Anderson localization, Bloch oscillations, electromagnetically induced transparency, and Zener tunneling [19–22]. Also, the quantum control techniques, which have been extensively studied in quantum metrology and computation [23–26], could also be implemented in photonic devices due to the same analogue. For example, the quantum adiabatic population transfer, which has been used in atomic state control [27–30], are generalized in the PIC to realize robust and broadband photonic devices, such as the long-pass filter [31–33], polarization rotators [34, 35],

broadband frequency conversion [36], mode multiplexer [37]and beam splitters [38].

In this paper, an adiabatic band-pass filter (ABPF) with a wide-band flat-top transmission is designed according to the coherent adiabatic passage technique. The filter consists of an asymmetric coupler with a modulated gap while the modulation period is chirped. By properly engineering the parameters of the device, the light input to one of the coupled waveguides can be transferred to the neighbor waveguide adiabatically, if its wavelength is located in a certain band. This spatial adiabatic tunneling passage is an optical analog of the temporal adiabatic state evolution in atomic systems [27–30]. The adiabatic mechanism promises the devices with high efficiency and robustness against the structural variations, such as the gap and the width of waveguides, therefore the proposed device is feasible for practical experiments. The chirped modulation studied in this work is different from the tapered gap or width in other adiabatic photonic designs, thus our work also provides an alternative way to manipulate the photons in PIC.

II. THE MODEL AND PRINCIPLE

The proposed ABPF is shown in Fig. 1(a), which is made by an asymmetric waveguide coupler. When light input from port 1, the signal with wavelengths in a selected band can couple to the other waveguide and will be dropped by the port 3, while the photons with the remaining wavelengths will directly exit from port 2. So the ports 2 and 3 can be used as a band-stop and band-pass filter, respectively. To suppress the direct light coupling between two waveguides for the wavelengths outside the bandwidth, which essentially becomes the stray light background of the filter, we choose the asymmetric sin-
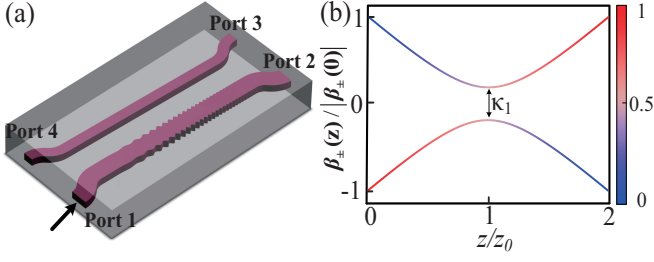
Figure 1. (a) The schematic illustration of the adiabatic filter. The core component is an asymmetric coupler made by silicon with a chirped modulation gap. Here, the geometry in z-direction is re-scaled for better illustration of the modulated gap. (b) The propagation wave-vector for the eigenmodes of the asymmetric coupler versus the propagation distance z in the rotating coordinate. The κ_1 corresponding to the amplitude of the modulated coupling coefficient (see main text). The different colors represent the energy weights of the eigenmodes of the coupler in the narrower waveguide.

gle mode waveguide coupler, so that the wave-numbers of the fundamental modes (β_1 and β_2) in two waveguides are different. Then, a periodic modulation of the gap is introduced to compensate the dispersive phase mismatching between the waveguides, thus the light with the wavelengths satisfying certain conditions for adiabatic conversion will be dropped at port 3. At the input side, because two waveguides are sufficiently separated that the light input from one waveguide can be regarded as an incidence in the form of an eigenmode of the coupler, so does the light at the output side. From the mode conversion point of view, the ABPF is essentially a wavelength-dependent mode converter.

According to the coupled mode theory, the dynamics of the light propagating in the two waveguides satisfy

$$\frac{d}{dz}E_1(z) = -i\beta_1(z)E_1(z) - i\kappa(z)E_2(z), \quad (1)$$

$$\frac{d}{dz}E_2(z) = -i\beta_2(z)E_2(z) - i\kappa(z)E_1(z), \quad (2)$$

where $E_j(z)$ is the amplitude of the electric field in the j-th waveguide and $\kappa(z)$ is the coupling coefficient between waveguides. Introducing the slowly varying amplitudes $a_j(z) = E_j(z)e^{-i\beta_j(z)z}$ ($j = 1, 2$), the coupled mode equations becomes

$$\frac{d}{dz}a_1(z) = -i\kappa(z)a_2(z)e^{-i\Delta\beta(z)z}, \quad (3)$$

$$\frac{d}{dz}a_2(z) = -i\kappa(z)a_1(z)e^{i\Delta\beta(z)z}, \quad (4)$$

with $\Delta\beta(z) = \beta_1(z) - \beta_2(z)$. According to our assumption $\Delta\beta \gg \kappa$, so the coupling between the two waveguides are strongly suppressed due to the fast varying phase $e^{\pm i\Delta\beta(z)z}$.

When introduces the modulation of the gap between the waveguides, i.e. the gap $g(z) = g_0 + \Delta g(z)$, the coupling coefficient $\kappa(z)$ between the waveguide could be modulated as well, where g_0 is the average gap and $\Delta g(z)$ is the modulation of the gap. For the weak perturbations $\Delta g(z) \ll \lambda$, where λ is the wavelength, the $\beta_i(z)$ can be treated as a constant along the waveguide, and we can approximate the modulated coupling coefficient to the leading order as

$$\kappa(z) = \kappa_0 + \kappa_1 \sin(\Omega(z)z), \quad (5)$$

where κ_0 is a constant coupling coefficient for the gap g_0 and κ_1 is the amplitude of the modulated coupling coefficient caused by the modulated gap. Then, for the coupled mode equation Eq. (3), the fast varying phase of the coupling term could be compensated by the modulation of κ_1 as

$$\frac{d}{dz}a_1 = -i\left[\kappa_0 + \frac{\kappa_1(e^{i\Omega(z)z} - e^{-i\Omega(z)z})}{2i}\right]e^{-i\Delta\beta z}a_2, \quad (6)$$

$$\frac{d}{dz}a_2 = -i\left[\kappa_0 + \frac{\kappa_1(e^{i\Omega(z)z} - e^{-i\Omega(z)z})}{2i}\right]e^{i\Delta\beta z}a_1. \quad (7)$$

When $\Delta\beta \approx \Omega(z)$ and $\kappa_0, \kappa_1 \ll \Delta\beta$, by neglecting the fast-varying term for the slowly varying amplitude approximation, we have

$$\frac{d}{dz}a_1 \approx -\frac{\kappa_1}{2}a_2 e^{i[\Omega(z) - \Delta\beta]z} \quad (8)$$

$$\frac{d}{dz}a_2 \approx \frac{\kappa_1}{2}a_1 e^{-i[\Omega(z) - \Delta\beta]z} \quad (9)$$

Considering a linear chirped modulation $\Omega(z) = \Omega_0 + Cz$, with C is the changing rate of the modulation frequency along the waveguide, the coupled equations in the rotating coordinates of $a_1' = a_1 e^{i(\Delta\beta - \Omega)/2}$ and $a_2' = a_2 e^{-i(\Delta\beta - \Omega)/2}$ can be written as

$$i\frac{d}{dz}\begin{bmatrix} a_1' \\ a_2' \end{bmatrix} = H_{\text{eff}}(z)\begin{bmatrix} a_1' \\ a_2' \end{bmatrix}, \quad (10)$$

with an effective Hamiltonian in the matrix form of

$$H_{\text{eff}}(z) = \frac{1}{2}\begin{bmatrix} -(\delta - 2Cz) & -i\kappa_1 \\ i\kappa_1 & \delta - 2Cz \end{bmatrix}, \quad (11)$$

as an spatial analog of the Eq. (10) to the Schrodinger's equation and $\delta = \Delta\beta - \Omega_0$.

As shown in Fig. 1(b), the eigenvalues of the $H_{\text{eff}}(z)$ as

$$\beta_{\pm}(z) = \pm\frac{1}{2}\sqrt{(2Cz - \delta)^2 + \kappa_1^2} \quad (12)$$

are plotted, which show an avoid crossing against z due to the chirped modulation, and the minimum difference of the eigenvalues is κ_1 when $z_0 = \delta/2C$. In the quantum adiabatic theorem, if a quantum system has no level crossings and evolves slowly enough, the system will remain in one of its eigenstates [39–41]. Similarly, when light propagates along z-axis, the system will follow the
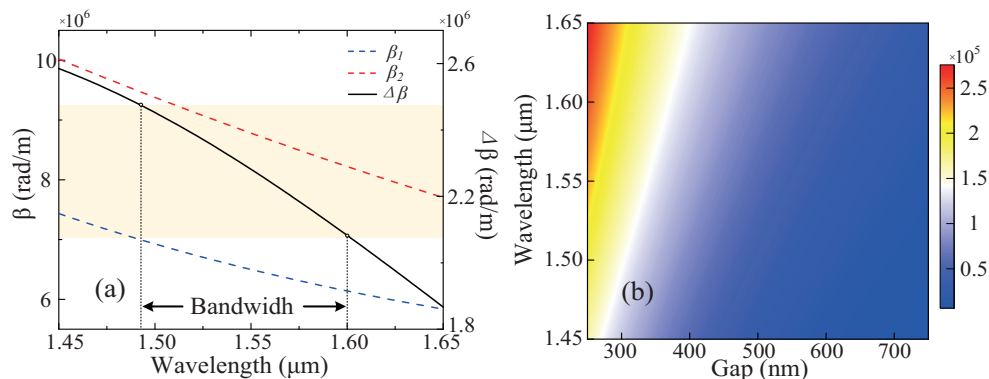
Figure 2. (a) The numerical simulated wave-vector of the modes in two waveguides versus wavelength with the waveguides cross-section dimension $220 \times 250\,\text{nm}$ and $220 \times 380\,\text{nm}$, respectively. The blue and red dash lines are the wave-vector of the waveguides, respectively. The black line is the difference of the wave-vectors in two waveguides. (b) The numerically simulated coupling coefficient κ versus the waveguide gap and wavelength.

mode evolution branches in Fig. 1(b) perfectly if the chirp is slow enough. In Fig. 1(b), the different colors represent the energy weights of the eigenmodes of the coupler in the narrower waveguide. The blue color represents the eigenmode that all the energy is in the wider waveguide when two waveguides are detuned sufficiently. So if the initially excited mode is the eigenmode represented by the blue color and the adiabatic evolution conditions are satisfied, the eigenmode represented by the red color will be the output at the position of $z = 2z_0$. According to the Landau-Zener tunneling theory[39], the maximum adiabatic mode conversion rate can be estimated by

$$\eta \approx 1 - e^{-\pi \kappa_1^2 / |4C|}. \tag{13}$$

Here, it is worth noting that the adiabatic conversion between the phase-mismatched waveguide modes originates from the spatially chirped modulation of the structure, which is an analog of the temporally chirped frequency modulation of the laser pulse in quantum control experiments[42, 43]. The mechanism studied here is different from the previously studied tapered geometry of the photonic structure [12, 44–46], which is similar to the temporal energy level shifting of a quantum system [27–30]. As is shown in Eq. (13), the maximum conversion rate is dependent on the dimensionless parameter $\kappa_1^2 / |4C|$. For a sufficient small C, the evolution of the optical modes in the coupler can be treated as adiabatic, and the light in one waveguide could be converted to the other one with the efficiency $\eta \to 1$. Although a smaller C results in higher conversion efficiency, it also makes a larger z_0, which means the footprint of the device will be larger.

In the above studies, we are only focusing on a single wavelength of the input light. Due to the geometry dispersion, the parameters κ_1, $\Delta\beta$, z_0 are wavelength dependent. Therefore, z_0 is different for different wavelengths that they will tunnel at different positions along

the waveguide. For the wavelengths tunneling at the position close to the ends of the asymmetric coupler, due to the evolution distance is not enough for the adiabatic mode evolution, the tunneling rate will be reduced. While for the wavelengths between them, the tunneling rate can approach 1, which means the device can be used as an optical filter with a broadband flat-top.

III. RESULTS

To test the proposed ABPF and directly illustrate the performances, we choose the silicon on insulator chip for numerical simulations, with the width of the waveguides are $w_1 = 250\,\text{nm}$ and $w_2 = 380\,\text{nm}$, respectively. The thickness of the silicon waveguides is $220\,\text{nm}$, and the upper cladding is silicon dioxide. The device is designed to operate at the wavelength around the telecom wavelength $1550\,\text{nm}$, with the refractive index of silicon about 3.48. According to the theoretical model, we set the gap between the waveguide as $g_0 = 500\,\text{nm}$ and the modulation as $|\Delta g| = 30\,nm$. Note that those parameters are practical since they are selected from the experiments [47].

By putting the parameters into the finite-element method (FEM) simulations (see Appendix), we obtain the $\kappa_0 = 6 \times 10^4$ and $\kappa_1 = 8.7 \times 10^3$ for $\lambda = 1550\,\text{nm}$. Due to the dispersion, the propagation constants and the coupling coefficients are related to wavelengths, as shown in Fig. 2(a). Therefore, for a certain range of Ω, as indicated by the yellow band in Fig. 2(a), only when the wavelengths that satisfy the phase matching condition of $\Delta\beta(\lambda) \approx \Omega$, the high efficient adiabatic conversion is possible. Therefore, the dispersion and the frequency range of the chirped modulation determines the bandwidth of the ABPF, as shown by the horizontal arrows in Fig. 2(a). Here, the $\Delta\beta \sim 2.2 \times 10^6\,\text{rad/m}$ corresponds to the modulation period of about $2.86\,\mu\text{m}$ for the phase

matching condition, thus the conditions $\Omega, \Delta\beta \gg \kappa_0, \kappa_1$ are satisfied. In the following, the numerical estimation of the wavelength-dependent transmittance of the waveguide is implemented, based on the FEM-calculated $\Delta\beta$ [Fig. 2(a)] and the coupling coefficients between waveguides for different wavelengths and gap [Fig. 2 (b)].

By numerically solving the coupled mode equations Eq. (2) without the slow amplitude varying approximation, the transmission spectrum and the power distribution along the waveguides are calculated, and the results are summarized in Fig. 3. In our configuration, the tunneling occurs at the middle of the coupler for the central wavelength of the band-pass filter. Because of the dispersion, the $\Delta\beta$ is smaller for larger wavelength, and the modulation frequency of gap increase linearly along the propagation direction in our configuration, thus the adiabatic tunneling will occur at a shorter propagation length for the larger wavelength. Although the Eq. (10) determine the dynamics of the system primarily, the high frequencies terms in the right side of the Eq. (7) will result in an additional high-frequency jitter on the transmission, as we can see from Figs. 3(b)-(d). The jitter will accordingly affect maximal transmission. To reduce the high-frequency jitter, a large Ω at the end of the coupler is suitable, moreover, according to the Eqs. (11)-(13), smaller C is expected to maximize the transmission. Both two considerations require a long device. To balance the length of the device and the maximum tunneling rate, we set $C = 10^7\,\mathrm{m}^{-2}$ and $L = 20\,\mathrm{mm}$. In addition to the small slope of the black line shown in Fig. 2(a), finally, a flat-top band-pass filter with a full width at half maximum (FWHM) bandwidth of $110\,\mathrm{nm}$ is obtained and the highest transmission is about 99.9%. The extinction ratio is about $20\,\mathrm{dB}$, as is shown in the red lines of Fig. 3(a).

Therefore, the numerical simulations confirm that chirped modulation of the gap between asymmetry waveguide coupler could be used for adiabatic wavelength-dependent mode conversion, which realizes a flat-top band-pass filter with large bandwidth and high efficiency. However, limited by the adiabatic criteria, the cost is the large size of the device. Although the fabrication of such a long device is not a challenge today, the device is still much longer than the general integrated optical devices. To reduce the length of the device and to tune the bandwidth without the influence the conversion efficiency, another parameter dimension of the device should be introduced. As we can see from Figs. 3(b)-(d) that for a specific wavelength the coupling happens mainly in a short length of the coupler about $5\,\mathrm{mm}$. At the other region, the further away from the coupling region, the larger the effective difference of propagation constant $\Delta\beta' = \Delta\beta - \Omega_0 - 2Cz$ is, which means the coupling is weaker. In the regions, the adiabatic condition can be relatively relaxed, so one way to reduce the length of the device is reducing the coupling coefficient κ_1, as
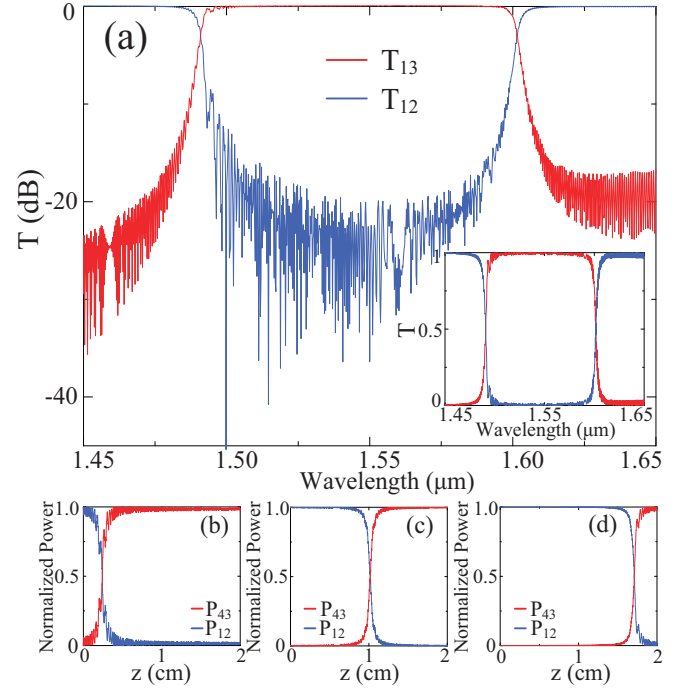

Figure 3. (a) The transmission spectra of the device. The FWHM bandwidth is about $110\,\mathrm{nm}$ with the extinction ratio about $20\,\mathrm{dB}$. The inset shows the transmission spectrum in linear type. (b-d) The normalized power distribution along the waveguides of the ABPF with the different wavelengths of $1590\,\mathrm{nm}$, $1550\,\mathrm{nm}$ and $1510\,\mathrm{nm}$, respectively. The red and blue lines are the transmission of T_{13} and T_{12}, respectively.

shown in Eq. (10). For the wavelengths of which coupling occurs in the regions, the mode conversion efficiency will be affected, so the bandwidth of the device is reduced either. Because κ_1 is proportional to the Δg, to reduce the coupling coefficient κ_1, we introduce an additional Gaussian modulation of Δg, i.e. the apodization technique [47, 48], the coupling coefficient between waveguides becomes

$$\kappa(z) = \kappa_0 + \kappa_1 e^{-(z-z_0)^2/\zeta^2}\sin(\Omega z), \qquad (14)$$

with the parameter ζ controls the width of the Gaussian function. By applying the slowly varying amplitude approximation the same as preceding analyses, the effective Hamiltonian becomes

$$H_{\mathrm{eff}}(z) = \frac{1}{2}\begin{bmatrix} -(\delta - 2Cz) & -i\kappa_1 e^{-\frac{(z-z_0)^2}{\zeta^2}} \\ i\kappa_1 e^{-\frac{(z-z_0)^2}{\zeta^2}} & \delta - 2Cz \end{bmatrix}. \qquad (15)$$

Figure 4(a) shows a typical transmission spectra of the apodized-ABPF. In this device, $\Omega_0 = 2.27 \times 10^6\,\mathrm{m}^{-1}$, $C = 4 \times 10^6\,\mathrm{m}^{-2}$, $\zeta = 1.1 \times 10^{-3}\,\mathrm{m}$, $z_0 = 2.2\,\mathrm{mm}$ and the length of the device is reduced to $4\,\mathrm{mm}$. Figures 4(b)-(d) are the corresponding power distribution along the waveguides with the different signal wavelengths of $1551\,\mathrm{nm}$, $1550\,\mathrm{nm}$ and $1549\,\mathrm{nm}$, respectively. As we can
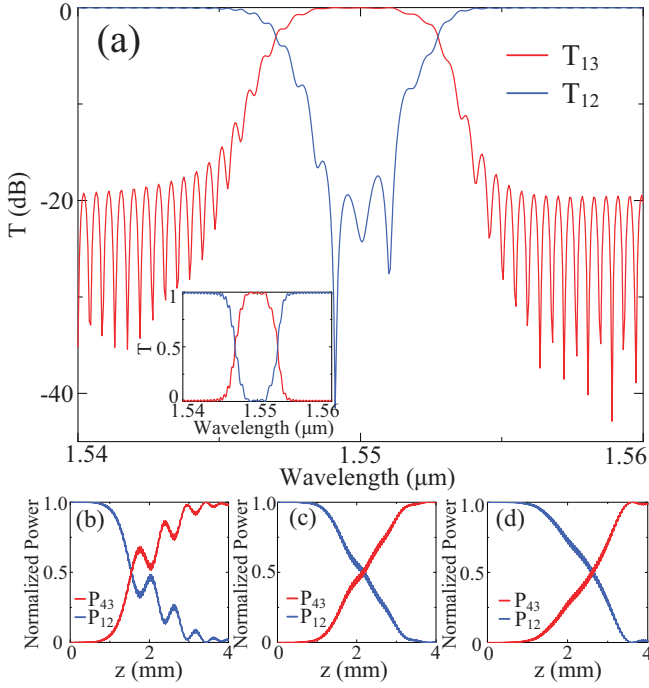
Figure 4. (a) The transmission spectrum of the device with an additional Gaussian modulation of the gap. The FWHM is about 6 nm with the extinction ratio about 20 dB. The inset shows the transmission spectrum in linear type. (b-d) The normalized power distribution along the waveguides of the ABPF with the different wavelengths of 1551 nm, 1550 nm and 1549 nm, respectively. The red and blue lines are the transmission of T_{13} and T_{12}, respectively.

Figure 5. (a)-(d) The tolerance of the device to the parameters of g_0, Δg, z_0 and the width ($w_1 = 250$ nm, $w_2 = 380$ nm) of two waveguides of the coupler. The black dash lines are the loss $1 - T$ for the center wavelength of 1550 nm. The red lines are the FWHM bandwidth of the transmission.

see from Fig. 4(a), the FWHM of the spectrum response is reduced to 6 nm with the flat-top about 3 nm. So by adding an additional Gaussian modulation of the Δg, we can control the bandwidth of the filter, but limited by the properties of adiabatic evolution, the bandwidth can hardly be smaller than 3 nm.

Lastly, we studied the robustness of the device performances against the variation of the device parameters. For an optical filter, in addition to the performance of high filtering efficiency and flat-top transmission, a device with a high tolerance can greatly improve the yield. In Fig. 5, the influence of the filter bandwidth and the transmittance of 1550 nm signal (to show the changing of the transmission clearly, we give the value of 1-T in the unit of dB) by the variations of g_0, Δg, z_0 and the width of the waveguides are numerically studied, with the other device parameters from Fig. 4. We found that when the gap between the asymmetric waveguides g_0 has a ± 50 nm error, the bandwidth of the transmission spectrum changes by only ± 0.5 nm. When Δg and z_0 have the error of ± 10 nm and $\pm 100\,\mu$m respectively, the bandwidth changes by about 1.2 nm and 0.03 nm. Because the dispersion and $\Delta\beta$ are sensitive to the variation of the width of the waveguides, the phase matching condition
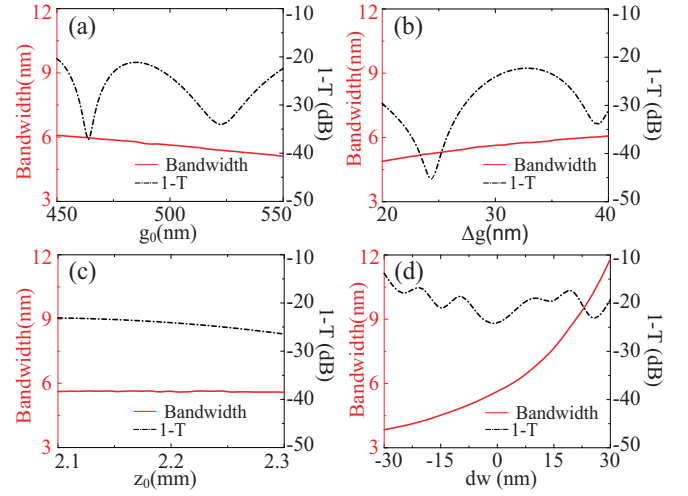
maybe breaks when width of the waveguides are changed. As is shown in Fig. 5(d), when the waveguides width has an error of ± 30 nm (the width of two waveguides change simultaneously), the bandwidth changes from 3.9 nm to 11.8 nm, which is relative large. However, according to the state of art of the nano-fabrication, the error of the waveguide width can be easily controlled within 10 nm. For the transmittance, as shown by the black dash lines in Fig. 5, the changing of the transmission of the center wavelength in all the situations mentioned above will be smaller than 10^{-2}.

As the results mentioned above, the adiabatic evolution promises a high-efficiency and robust mode conversion in principle, while the relatively large footprint of the device might also bring considerable propagation loss in practice, and the insertion loss of the filter will be affected. Especially for silicon-on-insulator (SOI) waveguide, the optical propagation loss is typically larger than 2 dB/cm [49]. Although we adapt the SOI as an example, the adiabatic principle is general and the scheme we proposed is also applicable to other optical materials. For example, the propagation loss as low as 0.54 dB/m for Silicon Nitride waveguide [50] and 2.7 dB/m for Lithium Niobate waveguide [51] has been demonstrated in experiments. So, by improving the nano-fabrication technology or changing the material, the optical loss can be reduced.

IV. CONCLUSION

In summary, a flat-top optical band-pass filter is proposed for the photonic integrated circuit. Based on the coupled asymmetric waveguide structure, the coupling

between the two waveguides with chirped modulation of the gap leads to the adiabatic mode conversion between the two waveguides. Due to the dispersion effect, only the light wavelength located in a certain range could be adiabatically dropped through the other waveguide, which causes a flat-top filtration function. For a typical device length of 20 mm, a full-width-half-maximum bandwidth of the filter is about 110 nm for telecom wavelength. By introducing apodization to the filter structure, a narrower bandwidth of 6 nm could be obtained with the length of the device about 4 mm. It is numerically verified that the performances of the proposed device are robust against geometry parameter uncertainties, thus our design is feasible for near future experiments. It is also expected that the chirp-modulation based adiabatic mode-conversion mechanism could be further exploited in the future studies of photonic integrated circuits.

Appendix: FEM simulations

In the paper, we use the finite-element method simulations to calculate the propagation constants β and the coupling coefficient $\kappa = \sqrt{\kappa_{12}\kappa_{21}}$, where κ_{pq} is calculated by the the numerical integration [52]:

$$\kappa_{pq} = \frac{\omega\varepsilon_0 \iint (\varepsilon_r - \varepsilon_{r,q})\boldsymbol{E}_p^*\boldsymbol{E}_q ds}{\iint (\boldsymbol{E}_p^* \times \boldsymbol{H}_p + \boldsymbol{E}_p \times \boldsymbol{H}_p^*) \cdot \boldsymbol{u}_z ds}$$

where p, q denotes two waveguides, ε_r denotes the relative dielectric constant distribution in the entire coupled waveguide and $\varepsilon_{r,q}$ denotes the relative dielectric constant distribution of waveguide q. By sweeping the wavlength and waveguide gap, we get the values of β and κ shown in Fig (2).

* clzou321@ustc.edu.cn

[1] W. Bogaerts, D. Taillaert, B. Luyssaert, P. Dumon, J. V. Campenhout, P. Bienstman, D. V. Thourhout, R. Baets, V. Wiaux, and S. Beckx, "Basic structures for photonic integrated circuits in silicon-on-insulator," Opt. Express **12**, 1583 (2004).

[2] R. Soref, "The past, present, and future of silicon photonics," IEEE J. Sel. Topics Quantum Electron. **12**, 1678 (2006).

[3] R. R. P. &. M. L. Vilson R. Almeida, Carlos A. Barrios, "All-optical control of light on a silicon chip," Nature **431**, 1081 (2004).

[4] C. Sun, M. T. Wade, Y. Lee, J. S. Orcutt, L. Alloatti, M. S. Georgas, A. S. Waterman, J. M. Shainline, R. R. Avizienis, S. Lin, B. R. Moss, R. Kumar, F. Pavanello, A. H. Atabaki, H. M. Cook, A. J. Ou, J. C. Leu, Y.-H. Chen, K. Asanović, R. J. Ram, M. A. Popović, and V. M. Stojanović, "Single-chip microprocessor that communicates directly using light," Nature **528**, 534 (2015).

[5] A. Politi, M. J. Cryan, J. G. Rarity, S. Yu, and J. L. O'brien, "Silica-on-silicon waveguide quantum circuits," Science **320**, 646 (2008).

[6] J. C. F. Matthews, A. Politi, A. Stefanov, and J. L. O'Brien, "Manipulation of multiphoton entanglement in waveguide quantum circuits," Nat. Photonics **3**, 346 (2009).

[7] S. Khasminskaya, F. Pyatkov, K. Slowik, S. Ferrari, O. Kahl, V. Kovalyuk, P. Rath, A. Vetter, F. Hennrich, M. M. Kappes, G. Goltsman, A. Korneev, C. Rockstuhl, R. Krupke, and W. H. P. Pernice, "Fully integrated quantum photonic circuit with an electrically driven light source," Nat. Photonics **10**, 727 (2016).

[8] X. Guo, C.-L. Zou, H. Jung, and H. X. Tang, "On-Chip Strong Coupling and Efficient Frequency Conversion between Telecom and Visible Optical Modes," Phys. Rev. Lett. **117**, 123902 (2016).

[9] B. Stern, X. Ji, Y. Okawachi, A. L. Gaeta, and M. Lipson, "Battery-operated integrated frequency comb generator," Nature **562**, 401 (2018).

[10] W. Bogaerts, P. Dumon, D. V. Thourhout, D. Taillaert, P. Jaenen, J. Wouters, S. Beckx, V. Wiaux, and R. G. Baets, "Compact wavelength-selective functions in silicon-on-insulator photonic wires," IEEE J. Sel. Topics Quantum Electron. **12**, 1394 (2006).

[11] W. Bogaerts, S. K. Selvaraja, P. Dumon, J. Brouckaert, K. D. Vos, D. V. Thourhout, and R. Baets, "Silicon-on-insulator spectral filters fabricated with cmos technology," IEEE J. Sel. Topics Quantum Electron. **16**, 33 (2010).

[12] E. S. Magden, N. Li, M. Raval, C. V. Poulton, A. Ruocco, N. Singh, D. Vermeulen, E. P. Ippen, L. A. Kolodziejski, and M. R. Watts, "Transmissive silicon photonic dichroic filters with spectrally selective waveguides," Nat. Commun. **9**, 3009 (2018).

[13] K. Yamada, T. Shoji, T. Tsuchizawa, T. Watanabe, J. ichi Takahashi, and S. ichi Itabashi, "Silicon-wire-based ultrasmall lattice filters with wide free spectral ranges," Opt. Lett. **28**, 1663 (2003).

[14] H. Qiu, H. Yu, T. Hu, G. Jiang, H. Shao, P. Yu, J. Yang, and X. Jiang, "Silicon mode multi/demultiplexer based on multimode grating-assisted couplers," Opt. Express **21**, 17904 (2013).

[15] M. Qiu, M. Mulot, M. Swillo, S. Anand, B. Jaskorzynska, A. Karlsson, M. Kamp, and A. Forchel, "Photonic crystal optical filter based on contra-directional waveguide coupling," Appl. Phys. Lett. **83**, 5121 (2003).

[16] Z. Qiang, W. Zhou, and R. A. Soref, "Optical add-drop filters based on photonic crystal ring resonators," Opt. Express **15**, 1823 (2007).

[17] T. Barwicz, M. A. Popovic, P. T. Rakich, M. R. Watts, H. A. Haus, E. P. Ippen, and H. I. Smith, "Microring-resonator-based add-drop filters in sin: fabrication and analysis," Opt. Express **12**, 1437 (2004).

[18] F. Xia, L. Sekaric, and Y. Vlasov, "Ultracompact optical buffers on a silicon chip," Nat. Photonics **1**, 65 (2007).

[19] X. Yang, M. Yu, D.-L. Kwong, and C. W. Wong, "All-optical analog to electromagnetically induced transparency in multiple coupled photonic crystal cavities," Phys. Rev. Lett. **102**, 173902 (2009).

[20] M. Segev, Y. Silberberg, and D. N. Christodoulides, "Anderson localization of light," Nat. Photonics **7**, 197 (2013).

[21] H. Trompeter, W. Krolikowski, D. N. Neshev, A. S. Desyatnikov, A. A. Sukhorukov, Y. S. Kivshar, T. Pertsch, U. Peschel, and F. Lederer, "Bloch oscillations and zener tunneling in two-dimensional photonic lattices," Phys. Rev. Lett. **96**, 053903 (2006).

[22] S. Longhi, "Quantum-optical analogies using photonic structures," Laser Photonics Rev. **3**, 243 (2009).

[23] C. H. Bennett and D. P. DiVincenzo, "Quantum information and computation," Nature **404**, 247 (2000).

[24] A. M. Childs, E. Farhi, and J. Preskill, "Robustness of adiabatic quantum computation," Phys. Rev. A **65**, 012322 (2001).

[25] V. Giovannetti, S. Lloyd, and L. Maccone, "Advances in quantum metrology," Nat. Photonics **5**, 222 (2011).

[26] P. A. Ivanov and D. Porras, "Adiabatic quantum metrology with strongly correlated quantum optical systems," Phys. Rev. A **88**, 023803 (2013).

[27] X. Chen, I. Lizuain, A. Ruschhaupt, D. Guéry-Odelin, and J. G. Muga, "Shortcut to adiabatic passage in two- and three-level atoms," Phys. Rev. Lett. **105**, 123003 (2010).

[28] A. Ruschhaupt, X. Chen, D. Alonso, and J. G. Muga, "Optimally robust shortcuts to population inversion in two-level quantum systems," New J. Phys. **14**, 093040 (2012).

[29] M. G. Bason, M. Viteau, N. Malossi, P. Huillery, E. Arimondo, D. Ciampini, R. Fazio, V. Giovannetti, R. Mannella, and O. Morsch, "High-fidelity quantum driving," Nat. Phys. **8**, 147 (2012).

[30] E. Torrontegui, S. Ibáñez, S. Martínez-Garaot, M. Modugno, A. del Campo, D. Guéry-Odelin, A. Ruschhaupt, X. Chen, and J. G. Muga, "Shortcuts to adiabaticity," in *Advances in Atomic, Molecular, and Optical Physics*, Vol. 62 (Elsevier, 2013) pp. 117–169.

[31] R. Menchon-Enrich, A. Llobera, J. Vila-Planas, V. J. Cadarso, J. Mompart, and V. Ahufinger, "Light spectral filtering based on spatial adiabatic passage," Light Sci. Appl. **2**, e90 (2013).

[32] X. Guo, C.-l. Zou, and H. X. Tang, "70 dB long-pass filter on a nanophotonic chip," Opt. Express **24**, 21167 (2016).

[33] H. Oukraou, L. Vittadello, V. Coda, C. Ciret, M. Alonzo, A. A. Rangelov, N. V. Vitanov, and G. Montemezzani, "Control of adiabatic light transfer in coupled waveguides with longitudinally varying detuning," Phys. Rev. A **95**, 023811 (2017).

[34] X. Xiong, C.-L. Zou, X.-F. Ren, and G.-C. Guo, "Integrated polarization rotator/converter by stimulated Raman adiabatic passage," Opt. Express **21**, 17097 (2013).

[35] X.-B. Xu, L. Shi, G.-C. Guo, C.-H. Dong, and C.-L. Zou, ""Möbius" microring resonator," Appl. Phys. Lett. **114**, 101106 (2019).

[36] X. Xiong, C.-L. Zou, X. Guo, H. X. Tang, X.-F. Ren, and G.-C. Guo, "Broadband frequency conversion and area law in tapered waveguides," OSA Continuum **1**, 1349 (2018).

[37] S. Yerolatsitis, I. Gris-Sánchez, and T. A. Birks, "Adiabatically-tapered fiber mode multiplexers," Opt. Express **22**, 608 (2014).

[38] X. Chen, R. D. Wen, J. L. Shi, and S. Y. Tseng, "Compact beam splitters in coupled waveguides using shortcuts to adiabaticity," J. Opt. **20** (2018).

[39] C. Zener, "Non- Adiabatic Crossing of Energy Levels." Proc. Royal Soc. Lond. A **137**, 696 (1932).

[40] T. Kato, "On the adiabatic theorem of quantum mechanics," J. Phys. Soc. Jpn. **5**, 435 (1950).

[41] B. Simon, "Holonomy, the quantum adiabatic theorem, and berry's phase," Phys. Rev. Lett. **51**, 2167 (1983).

[42] G. P. Djotyan, J. S. Bakos, Z. Sörlei, and J. Szigeti, "Coherent control of atomic quantum states by single frequency-chirped laser pulses," Phys. Rev. A **70**, 063406 (2004).

[43] M. J. Wright, S. D. Gensemer, J. Vala, R. Kosloff, and P. L. Gould, "Control of ultracold collisions with frequency-chirped light," Phys. Rev. Lett. **95**, 063001 (2005).

[44] S. Longhi, G. Della Valle, M. Ornigotti, and P. Laporta, "Coherent tunneling by adiabatic passage in an optical waveguide system," Phys. Rev. B **76**, 201101 (2007).

[45] K. Chung, T. J. Karle, M. Rab, A. D. Greentree, and S. Tomljenovic-Hanic, "Broadband and robust optical waveguide devices using coherent tunnelling adiabatic passage," Opt. Express **20**, 23108 (2012).

[46] H. S. Hristova, A. A. Rangelov, G. Montemezzani, and N. V. Vitanov, "Adiabatic three-waveguide coupler," Phys. Rev. A **93**, 033802 (2016).

[47] A. D. Simard, N. Belhadj, Y. Painchaud, and S. Larochelle, "Apodized silicon-on-insulator bragg gratings," IEEE Photon. Technol. Lett. **24**, 1033 (2012).

[48] M. Ma, Z. Chen, H. Yun, Y. Wang, X. Wang, N. A. Jaeger, and L. Chrostowski, "Apodized spiral bragg grating waveguides in silicon-on-insulator," IEEE Photon. Technol. Lett. **30**, 111 (2018).

[49] Y. A. Vlasov and S. J. McNab, "Losses in single-mode silicon-on-insulator strip waveguides and bends," Optics Express **12**, 1622 (2004).

[50] X. Ji, F. A. S. Barbosa, S. P. Roberts, A. Dutt, J. Cardenas, Y. Okawachi, A. Bryant, A. L. Gaeta, and M. Lipson, "Ultra-low-loss on-chip resonators with sub-milliwatt parametric oscillation threshold," Optica **4**, 619 (2017).

[51] M. Zhang, C. Wang, R. Cheng, A. Shams-Ansari, and M. Loncar, "Monolithic Ultrahigh-Q Lithium Niobate Microring Resonator," Optica **4**, 1536 (2017).

[52] K. Okamoto, *Fundamentals of optical waveguides* (Academic press, 2006).